J Solid State Electrochem (2010) 14:651–657
DOI 10.1007/s10008-009-0835-0

ORIGINAL PAPER

The preparation of PANI/CA composite electrode material for supercapacitors and its electrochemical performance

Hongfang An · Ying Wang · Xianyou Wang · Na Li · Liping Zheng

Received: 18 January 2009 / Revised: 4 March 2009 / Accepted: 20 March 2009 / Published online: 1 April 2009

Abstract Polyaniline (PANI)/carbon aerogel (CA) composite electrode materials were prepared by chemical oxidation polymerization. The morphology of PANI/CA composite was examined by scanning electron microscopy. The results showed that PANI was uniformly deposited onto the surface of porous CA and filled big inner pores of the CA. Electrochemical performance of the composite electrode was studied by cyclic voltammograms and galvanostatic charge/discharge measurements. The results indicated that the PANI/CA composite electrode had much better electrochemical performance, high reversibility, and high charge/discharge properties than CA. Moreover, the results based on cyclic voltammograms showed that the composite material has a high specific capacitance of 710.7 F g^{-1}, while the capacitance of CA electrode was only 143.8 F g^{-1}. Besides, the supercapacitor using the PANI/CA composite as electrode active material showed a stable cycle life in the potential range of −0.2–0.8 V.

Keywords Supercapacitor · Carbon aerogel · Polyaniline · Composite

H. An · X. Wang (✉) · N. Li · L. Zheng
School of Chemistry,
Key Laboratory of Environmentally Friendly Chemistry and Applications of Minister of Education, Xiangtan University,
Xiangtan, Hunan 411105, China
e-mail: wxianyou@yahoo.com

Y. Wang
School of Chemical Engineering and Pharmacy,
Wuhan Institute of Technology,
Wuhan, Hubei 430073, China

Introduction

Recently, electrochemical capacitors have attracted considerable attention for use in high power energy storage devices, such as the application to electric vehicles, pulse power, and backup sources [1]. The energy storage of supercapacitors based on double layer is the accumulation of ionic charges which occur at the electrode/electrolyte interface, so the high surface area and the porosity of the electrode active material are the basic requirements to achieve high specific capacitance. Carbon materials have been considered as a good candidate for the double-layer capacitance because of its high specific area, long cycle life, cheap price, and wide use in aqueous and nonaqueous solvents [2]. Usually, the carbon materials only possess double-layer capacitance, while metal oxide and conducting polymer all possess Faradic capacitance. Generally, the Faradic capacitance is ten to 100 times higher than double-layer capacitance [3]. In order to further enhance the specific capacitance of supercapacitors based on carbon materials, much attention has been placed on composite electrode materials in which the capacitance is the combination of double-layer capacitance and Faradic capacitance. The composite electrode materials usually consist of carbon materials and metal oxide [4, 5] or conducting polymer [6–9]. Conducting polymers have been used as redox supercapacitor electrodes in which energy is stored by the reversible electrochemical n- or p-type doping–undoping reaction:

$$\mathrm{p-doping}:(\mathrm{Polymer}) + \mathrm{yA}^- \rightarrow [(\mathrm{Polymer})\mathrm{y}^+\mathrm{yA}^-] + \mathrm{ye}^- \quad (1)$$

$$\mathrm{n-doping}:(\mathrm{Polymer}) + \mathrm{yC}^+ + \mathrm{ye}^- \rightarrow [(\mathrm{Polymer})\ \mathrm{y}^-\mathrm{yC}^+] \quad (2)$$

Polyaniline (PANI) is one of the promising conducting polymers in the application of supercapacitor electrode materials [10] due to its high conductivity, ease of preparation, and good environmental stability. It is reported that the specific capacitances of the supercapacitors using PANI-coated mesoporous activated carbon and microporous activated carbons as electrode active material are as high as 72 and 60 F g^{-1} [11]. Carbon aerogel is a kind of novel mesoporous carbon materials with an electrically conductive carbon network, a low density, and other interesting properties [12–14]. Talbi et al. reported that PANI was electrochemically synthesized on carbon polyacrylonitrile aerogel electrodes, and the specific capacitance of the composite reached as high as 240 F g^{-1} at a deposition time of 50 s [15].

In previous works, we studied preparation technology and electrochemical properties of carbon aerogel (CA) [16] and the composites of CA with RuO_2 [17] and MnO_2 [18]. In this paper, the PANI/CA composite was prepared by adsorption of aniline in the micropores of CA and, subsequently, chemical oxidation polymerized. The structural characterization and the electrochemical performance of the PANI/CA were investigated.

Experimental

Preparation of electrode active material

Materials

All the materials and chemical reagents were of analytical grade, such as resorcinol, formaldehyde, sodium carbonate, acetone, aniline, ethanol, ammonium peroxodisulfate, hydrochloric acid, and ammonia solution, which were obtained from commercial sources and directly used without any pretreatment. The water was deionized water.

Preparation of CA

CA was derived from pyrolysis of a resorcinol–formaldehyde gel. The procedure was reported in our previous study [16]. The molar ratio of formaldehyde (F) to resorcinol (R) was held at a constant value of 2. Na_2CO_3 (C) was added as the catalyst. During the preparation process, the R/C ratio was controlled to 1,500.

Preparation of the PANI/CA composite

The PANI-coated CA was prepared by adsorption of aniline on CA followed by chemical polymerization [11] with ammonium peroxodisulfate, and its synthesis route of PANI/CA composite is schematically represented in Fig. 1. The adsorption of aniline on carbon aerogel was accomplished by stirring 0.2 g of carbon aerogel in 40 mL of E_tOH solution including 20 mL aniline for 24 h under 5 °C. The aniline-loaded CA was separated from the solution by centrifugation. The polymerization of aniline adsorbed on CA was carried out by dispersing and stirring aniline-loaded CA in 50 mL of 0.18 M ammonium peroxodisulfate aqueous solution for 3 h under 5 °C. The dispersion was filtrated and the separated CA was washed with 1 M HCl and 0.1 M NH_3 aqueous solution several times. Eventually, the PANI/CA composites were obtained by washing with deionized water until the filtrate was litmusless. The PANI/CA composites were dried under vacuum for 12 h at 50 °C.

Measurement techniques of structural characterization

Scanning electron microscopy (SEM) was also used to study the surface structure of the samples by Hitachi S-3500N. BET specific surface areas were determined from N_2 adsorption/desorption isotherms, which were obtained by a Quantachrome NOVA 3200. The estimations of mesopore-specific surface areas and pore size distributions were carried out according to the BJH method.

Preparation of the PANI/CA composite electrode and electrochemical measurements

The mixture containing 80 wt.% PANI/CA composite, 10 wt.% acetylene black, and 10 wt.% polytetrafluoroethylene was well mixed, and then pressed onto a stainless steel grid (1.6×10^6 Pa) that used as a current collector (area was 1.5 cm^2), and then dried at 353 K for 12 h . The electrochemical performances of the prepared electrodes were characterized by cyclic voltammogram (CV) and

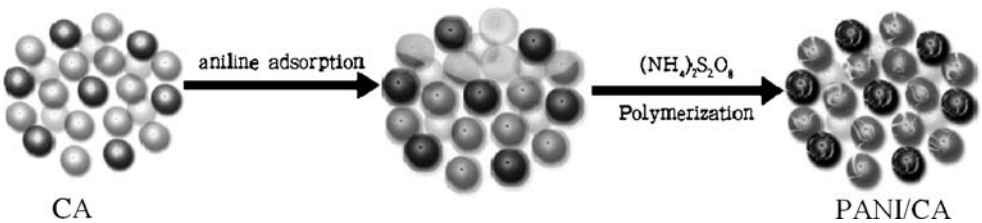

Fig. 1 Schematic preparing process of PANI on the surface of carbon aerogel

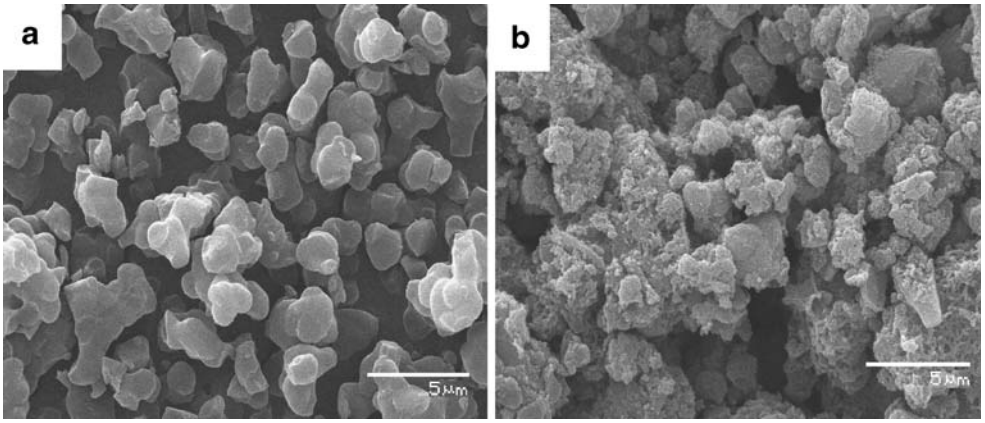

Fig. 2 SEM photographs of CA (**a**) and PANI/CA (**b**)

charge/discharge tests. The used electrolyte was 1 M H_2SO_4 solution. The experiments were carried out using a three-electrode cell, in which the stainless steel grid and the saturated calomel electrode were used as counter and reference electrodes. The cyclic voltammogram and the charge/discharge measurements at constant current were performed by means of electrochemical analyzer systems, CHI660 (CH Instruments, USA). The cycle life was carried out by potentiostat/galvanostat (BTS6.0, Neware, Guangdong, China) on button cell supercapacitors, and the symmetrical button cell supercapacitors were assembled according to the order of electrode–separator–electrode.

Results and discussion

Material characterization

The CA and PANI/CA composite materials were examined by SEM, and the typical results are shown in Fig. 2. CA was an amorphous material with a pearly network structure. It is seen from Fig. 2 that PANI is uniformly deposited onto the surface of porous CA and filled big inner pores of the CA.

Adsorption isotherm of N_2 gas was carried out in order to characterize the porous structure of the samples. Figure 3 shows the typical adsorption/desorption isotherm and the pore size distribution of PANI/CA composite at 77 K. The pore characteristics of CA and PANI/CA composite are shown in Table 1. In Fig. 3a, a hysteresis loop was observed, indicating that the composite had the structure of micropore and mesopore, and thus, the composite was beneficial to electrolyte ion movement. It can be found from Table 1 that the BET-specific surface area, pore volume, and average pore size of the composite all decreased after CA was coated by PANI, which ascribed to PANI blockage of the micropore in the CA.

Electrochemical characterization

Cyclic voltammogram is used in the determination of the electrochemical properties of the PANI/CA composite

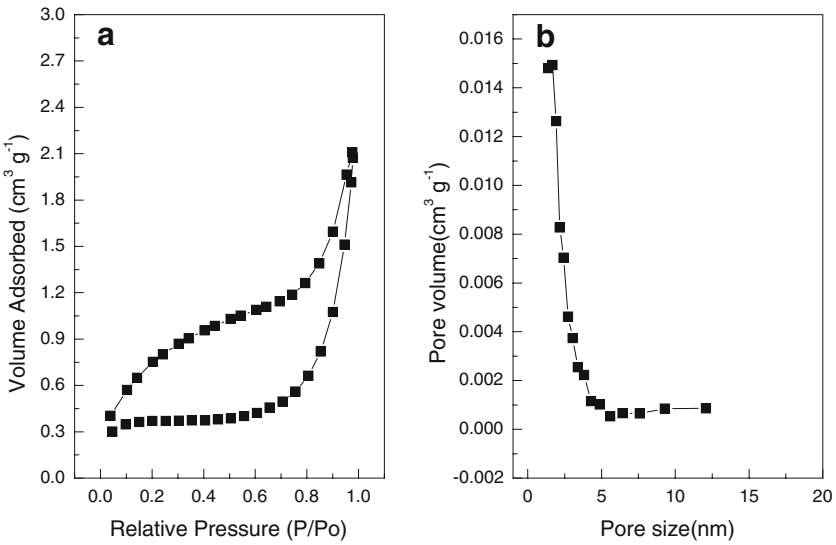

Fig. 3 Nitrogen adsorption isotherm at 77 K (**a**) and pore size distribution (**b**) of PANI/CA

Table 1 Pore characteristics of CA and PANI/CA

	BET-SSA[a] ($m^2\ g^{-1}$)	Pore volume ($cm^3\ g^{-1}$)	Average pore size(nm)
CA	469.432	0.049	1.677
PANI/CA	13.357	0.044	1.385

[a] Specific surface area evaluated by the BET method

electrodes. Cyclic voltammograms for the CA electrode and PANI/CA composite electrode are shown in Fig. 4. Figure 4 reveals that the capacitance characteristic of the PANI/CA composite electrode is distinct from that of the electric double-layer capacitance, which can generally produce a CV curve close to the ideal rectangular shape. Comparing the CVs in Fig. 4, it can be found that PANI/CA composite electrode has two couples of redox peaks, and the area surrounded by the CV curve is clearly larger than one of the CA electrode, indicating that the PANI/CA electrode has much more specific capacitance. Two redox peaks in Fig. 4 are attributed to the redox transition of PANI between a semiconducting state (leucoemeraldine form) and a conducting sate (polaronic emeraldine form) and the emeraldine–pernigraniline transformation [19]. Based on the CV, the capacitance was obtained from Eq. 3 [20]

$$C = \frac{Q}{V} = \int \frac{i\mathrm{d}t}{\Delta V} \tag{3}$$

where i is a sampled current, dt is a sampling time span, and $\triangle V$ is the total potential deviation of the voltage window.

Figure 5 shows cyclic voltammograms of the CA electrode and the PANI/CA electrode at different scan rates. The results measured from Fig. 5 are tabulated in Table 2. It can be found in Fig. 5 and Table 2 that the specific capacitance of the PANI/CA composite electrode increased obviously than one of the CA electrodes at every given scan rate. Although coating PANI on CA will decrease the specific surface area of PANI/CA electrode and result in the decrease of the double-layer capacitance, PANI on PANI/CA electrode can produce a very big pseudocapacitance. The resulted pseudocapacitance is so big that the PANI/CA electrode has still a big specific capacitance except for making up the loss of double-layer capacitance.

In order to gain a further understanding on the electrochemical performance of PANI/CA composite materials, the comparison of galvanostatic charge/discharge curves for the CA electrode and PANI/CA composite electrode is shown in Fig. 6. The galvanostatic charge/discharge curve of CA is almost linear, indicating that CA has only a double-layer capacitive behavior. In comparison, the charge/discharge curve of PANI/CA is not ideal linear, indicating that the specific capacitance of the composite electrode is composed of both the double-layer capacitance of CA and Faradic capacitance of PANI.

The charge/discharge curves of the PANI/CA composite electrodes measured at different current densities within a potential window (–0.2 to 0.8 V vs. SCE) are shown in Fig. 7. The specific capacitance can be calculated according to Eq. 4 [21], and the results are tabulated in Table 3.

$$C_{\mathrm{m}} = \frac{C}{m} = \frac{I \times t}{\Delta V \times m} \tag{4}$$

Here, C_{m} is the specific capacitance, I is the charge/discharge current, $\triangle V$ is the range of the charge/discharge, t is the discharge time, and m is the mass of active material within the electrode. As being seen from Table 3, the specific capacitance will decrease with the increase of charge/discharge current density, but the specific capacitance for PANI/CA electrode is apparently bigger than one of the CA electrode at every given current density, which is in good agreement with the results of cyclic voltammograms in Table 2.

The impedance responses (Nyquist plots) of the CA electrode and PANI/CA composite electrode are shown in Fig. 8. In all cases, Nyquist plots consisted of a semicircle at high frequency and a straight line in the low-frequency region. The semicircle results from the parallel combination of resistance and capacitance, and the linear region is because of Warburg impedance. In the low-frequency region, the straight line part leans more towards the imaginary axis and this indicates good capacitive behavior. The bulk resistance (0.548 Ω) of the PANI/CA composite is slightly larger than CA (0.521 Ω), and the reason is maybe the average pore size in Table 1 is decreased from CA to

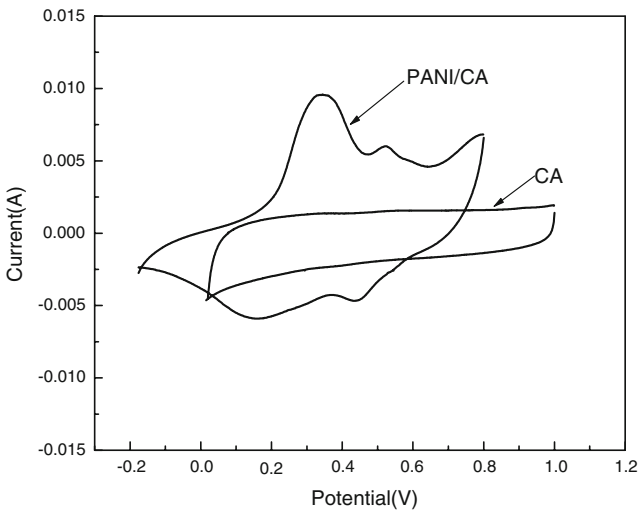

Fig. 4 Cyclic voltammograms for CA and PANI/CA electrodes

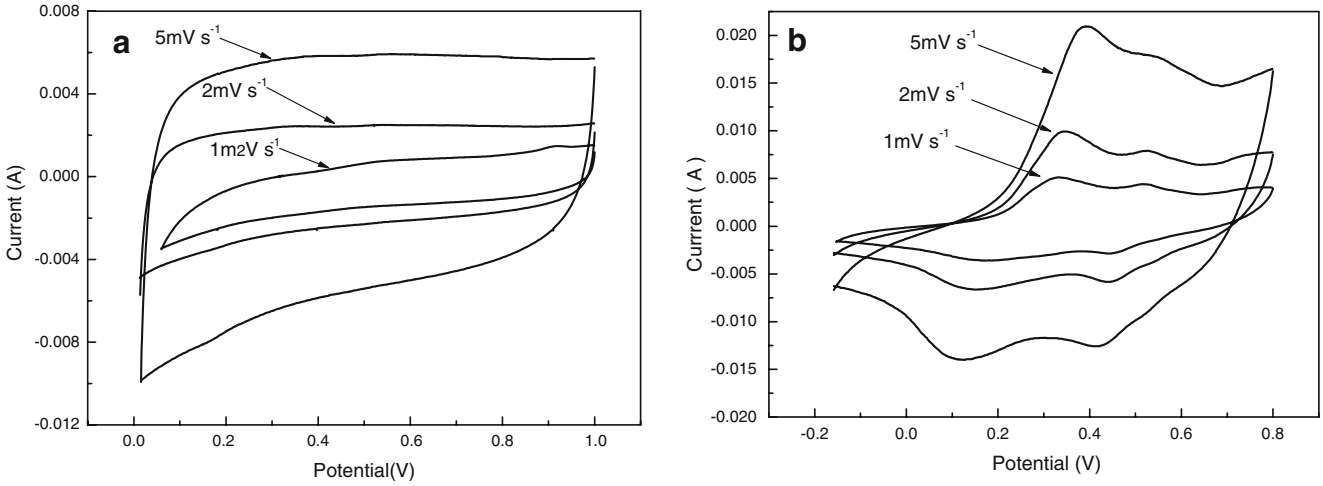

Fig. 5 Cyclic voltammograms for **a** CA and **b** PANI/CA at different scan rates

PANI/CA composite and ion transfer rate in the pore of PANI/CA becomes slower.

Table 4 presented the specific capacitance at different frequencies based on Fig. 8. The capacitance were obtained from Eq. 5 [22]

$$C = -\frac{1}{2\pi f \mathrm{SZ''}}. \tag{5}$$

Here, C is the specific capacitance, f is the frequency, Z'' is the imaginary part in impedance, and S is the geometrical area of the electrode. It is found that the specific capacitance of the PANI/CA composite is higher than CA in the different frequency regions.

The cycle life of the CA and the PANI/CA supercapacitors is illustrated in Fig. 9. As shown in Fig. 9, the CA and PANI/CA supercapacitors have demonstrated a very long cycle life under shallow depths of discharge, but the specific capacitance (39.6 F g^{-1}) of the CA supercapacitors is lower than the PANI/CA composite (133.3 F g^{-1}). Besides, the loss of capacitance of the PANI/CA supercapacitors was large at the beginning of the cycle, but the curve became smoother with increasing of cycle number. After 200 consecutive cycles, the capacitance of the PANI/CA supercapacitors fixed at a steady value; it was still at 76 F g^{-1} even though it was worked 1,000 cycles, which is higher than the results reported by Tamai [11] (70 F/g after 200 cycles). Such a low decrease in specific capacitance after the long charge/discharge cycle indicates the high stability of the composite and its potential prospect as an electrode active material for long-term supercapacitors applications.

Figure 10 is the Ragone plot of the CA and the PANI/CA supercapacitors. Energy density and power density are calculated using Eqs. 6 and 7 [23]

$$E = \frac{1}{2}C(\Delta V)^2 \tag{6}$$

$$P = \frac{I\Delta V}{2m} \tag{7}$$

Table 2 Specific capacitance (farad per gram) of CA and PANI/CA within different scan rates

	10mV s^{-1}	5mV s^{-1}	2mV s^{-1}	1mV s^{-1}
CA	107.2	120.5	129.7	143.8
PANI/CA	411.6	517.3	613.4	710.7

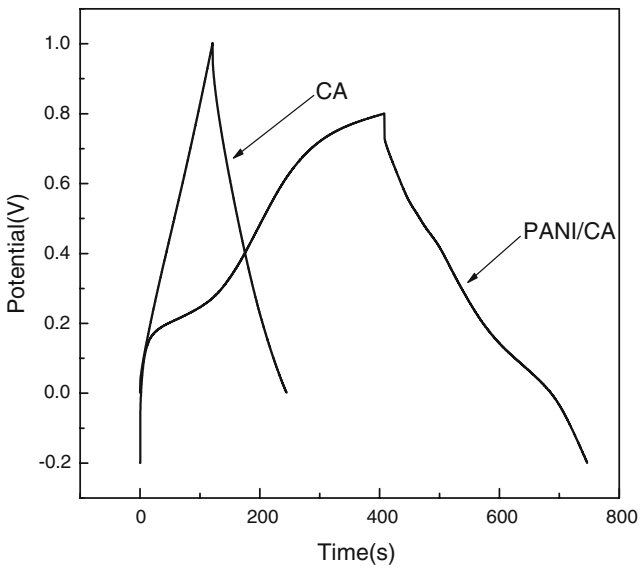

Fig. 6 The charge/discharge curves of PANI/CA electrodes and CA at 1 A g^{-1}

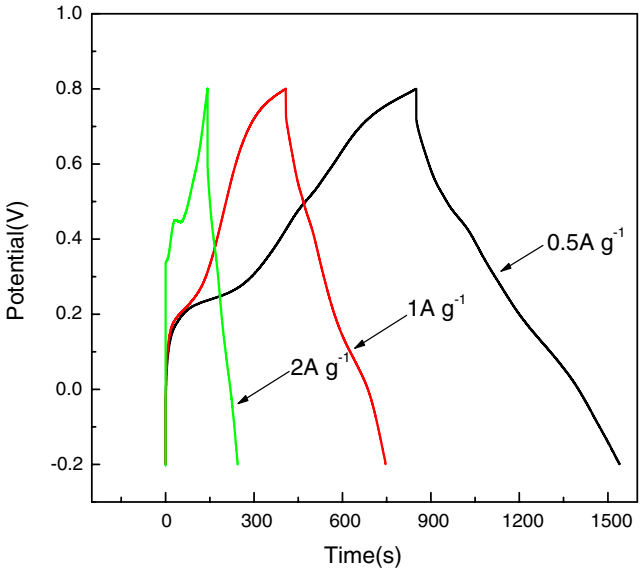

Fig. 7 The charge/discharge curves of PANI/CA electrodes at different current densities

Table 3 Specific capacitance (farad per gram) of CA and PANI/CA within different current densities

	2A g^{-1}	1A g^{-1}	0.5A g^{-1}
CA	99.6	123.6	127.8
PANI/CA	205.8	338.4	344.9

Table 4 Specific capacitance (farad per square centimeter) of CA and PANI/CA within different frequencies

	30Hz	3Hz	0.3Hz	0.03Hz
CA	0.058	0.381	0.747	1.06
PANI/CA	0.0591	0.397	1.256	2.11

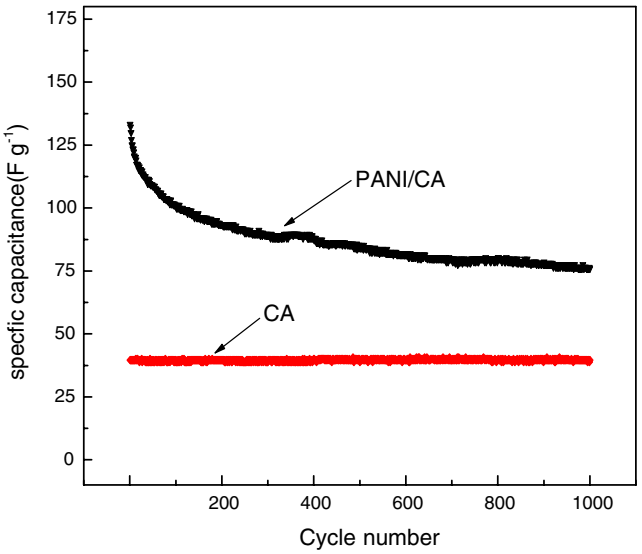

Fig. 9 Cycle life of carbon aerogel and PANI/CA supercapacitor under constant current (5 mA)

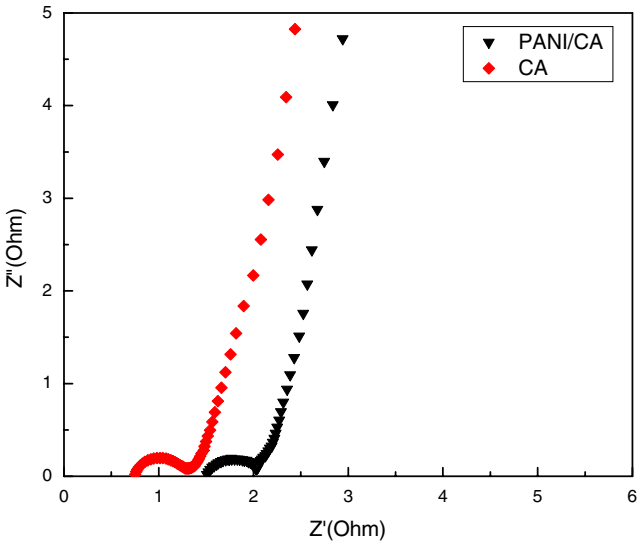

Fig. 8 Nyquist plot of CA and PANI/CA composite electrodes

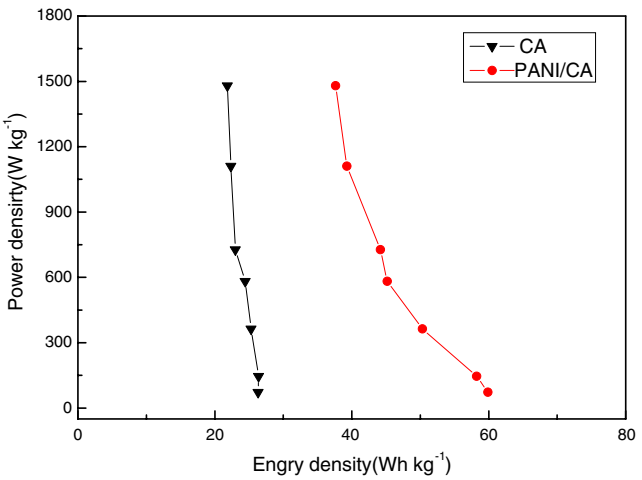

Fig. 10 Ragone plot of the CA and PANI/CA supercapacitors

Where C is the capacitance of the capacitor, and it is calculated according to Eq. 4; I, $\triangle V$, and m represent discharge current, range of the charge/discharge, and mass of active materials, respectively. It can be found that the CA and the PANI/CA supercapacitors achieved an energy density of 26.4 and 58.25 W h kg^{-1}, respectively. Besides, the supercapacitors based on both the CA and the PANI/CA composite have an excellent power performance. However, with the increasing of the power density, the energy density of the PANI/CA supercapacitors decreased slightly faster than that of the CA supercapacitors because the speed of the redox reactions within the PANI is not as fast as the formation of the electric double layer in the CA electrode.

Comparing the results of cyclic voltammogram and charge/discharge and impedance measurements, it can be seen that the specific capacitance of the PANI/CA composite is markedly higher than CA whether based on electrode or supercapacitor measurement. Therefore, surface modification of PANI is an effective way to improve the electrochemical performance of CA and increase its specific capacitance.

Conclusions

PANI/CA was prepared by chemical polymerization of adsorbed aniline and characterized for application to electrochemical capacitors. The specific surface area of PANI/CA will decrease due to coating PANI on the surface of CA. However, incorporation of PANI can increase dramatically the charge storage capacity, and the specific capacitance of PANI/CA electrode reached to 710.7 F g^{-1} through CV test which is five times higher than that of a CA electrode. In addition, the PANI/CA supercapacitors have stable electrochemical properties and a long cycle life. The specific capacitance of supercapacitors based on the PANI/CA composite reached 133.3 F g^{-1}, and its specific capacitance was higher than CA supercapacitors after 1,000 cycles. The energy density of the PANI/CA supercapacitors is apparently higher than one of CA supercapacitors. All these indicate that the PANI/AC composite is a promising electrode material for supercapacitors.

Acknowledgments This work was financially supported by the National Natural Science Foundation of China (Grant no. 20871101) and the Key Project of Education Department of Hunan Province Government (Grant no. 08A067).

References

1. Portet C, Taberna PL, Simon P et al (2005) Electrochim Acta 50:417. doi:10.1016/j.electacta.2005.01.038
2. Kwang SR, Young GL, Kang MK et al (2005) Synth Met 153:89. doi:10.1016/j.synthmet.2005.07.167
3. Peng Ch, Zhang ShW, Daniel J et al (2008) Prog Nat Sci 18:777. doi:10.1016/j.pnsc.2008.03.002
4. Chen WC, Hu CC, Wang CC (2004) J Power Sources 125:292. doi:10.1016/j.jpowsour.2003.08.001
5. Kalakodimi PR, Norio M (2004) Electrochem Solid-State Lett 7–11:425
6. Selvakumar M, Bhat DK (2008) J Appl Polym Sci 107:2165. doi:10.1002/app. 27166
7. Kima JH, Lee YS, Sharma AK et al (2006) Electrochim Acta 52:1727. doi:10.1016/j.electacta.2006.02.059
8. Xing W, Zhuo SP, Cui HY et al (2007) Mater Lett 61:4627. doi:10.1016/j.matlet.2007.02.062
9. Muthulakshmi B, Kalpana D, Pitchumani S et al (2006) J Power Sources 158:1533. doi:10.1016/j.jpowsour.2005.10.013
10. Gupta V, Miura N (2006) Mater Lett 60:1466. doi:10.1016/j.matlet.2005.11.047
11. Tamai H, Hakoda EM, Shiono ET et al (2007) J Mater Sci 42:1293. doi:10.1007/s10853-006-1059-7
12. Liu N, Zhang ST, Fu R et al (2006) Carbon 44:2430. doi:10.1016/j.carbon.2006.04.032
13. Kim SJ, Hwang SW, Hyun SH (2005) J Mater Sci 40:725. doi:10.1007/s10853-005-6313-x
14. Baumann TF, Worsley MA, T Han YJ et al (2008) J Non-Crystalline Solids 354:3513. doi:10.1016/j.jnoncrysol.2008.03.006
15. Talbi H, Just P-E, Dao LH (2003) J Appl Electrochem 33:465. doi:10.1023/A:1024439023251
16. Li J, Wang XY, Huang QH (2006) J Power Sources 158:784. doi:10.1016/j.jpowsour.2005.09.045
17. Li J, Wang XY, Huang QH (2007) J Appl Electrochem 37:1129. doi:10.1007/s10800-007-9372-7
18. Li J, Wang XY, Huang QH et al (2006) J Power Sources 160:1501. doi:10.1016/j.jpowsour.2006.02.045
19. Hu CC, Lin JY (2002) Electrochim Acta 47:4055. doi:10.1016/S0013-4686(02)00411-5
20. Kima JH, Lee YS, Sharma AK et al (2006) Electrochim Acta 52:1727. doi:10.1016/j.electacta.2006.02.059
21. Wang YG, Li HQ, Xia YY (2006) Adv Mater 18:2619. doi:10.1002/adma.200600445
22. Ryu KS, Lee YG, Kim KM et al (2005) Synth Met 153:89. doi:10.1016/j.synthmet.2005.07.167
23. Xue Y, Chen Y, Zhang ML et al (2008) Mater Lett 62:3884. doi:10.1016/j.matlet.2008.05.014